Met. Mater. Int., Vol. 21, No. 2 (2015), pp. 286~294
doi: 10.1007/s12540-015-4148-9

Experimental Determination of Interfacial Energies for Solid Sn in Equilibrium with Sn-Mg-Zn Liquid

Yemliha Altıntas[1], Esra Öztürk[2], Sezen Aksöz[3], Kâzım Keşlioğlu[4,*], and Necmettin Maraşlı[5]

[1]Department of Materials Science and Nanotechnology, Faculty of Engineering and Natural Science, Abdullah Gül University, Kayseri, Turkey
[2]Department of Physics, Faculty of Arts and Science, Kocaeli University, Kocaeli, Turkey
[3]Department of Physics, Faculty of Arts and Science, Nevşehir Hacı Bektaş Veli University, Nevşehir, Turkey
[4]Department of Physics, Faculty of Science, Erciyes University, Kayseri, 38039, Turkey
[5]Department of Metallurgical and Materials Engineering, Faculty of Chemical and Metallurgical Engineering, Yıldız Technical University, Davutpaşa-İstanbul, 34210, Turkey

(received date: 18 March 2014 / accepted date: 1 October 2014)

The equilibrated grain boundary groove shapes of solid Sn in equilibrium with Sn-Mg-Zn liquid were observed from a quenched sample by using a radial heat flow apparatus. The Gibbs-Thomson coefficient, solid-liquid interfacial energy and grain boundary energy of solid Sn were determined from the observed grain boundary groove shapes. The thermal conductivity of the eutectic solid phase for Sn-8.12 at% Mg-4.97 at% Zn alloy and the thermal conductivity ratio of the liquid phase to the solid phase for Sn-8.12 at% Mg-4.97 at% Zn alloy at eutectic temperature were also measured with a radial heat flow apparatus and a Bridgman-type growth apparatus, respectively. The Gibbs-Thomson coefficient, solid-liquid interfacial energy and grain boundary energy of solid Sn in equilibrium with Sn-Mg-Zn liquid were determined to be $(8.3 \pm 0.6)\times10^{-8}$ Km, $(118.5 \pm 14.2)\times10^{-3}$ J m^{-2} and $(225.1 \pm 29.3)\times10^{-3}$ J m^{-2} respectively from observed grain boundary groove shapes. A comparison of present results for solid Sn in the Sn-8.12 at% Mg-4.97 at% Zn alloy with the results obtained in previous works for similar solid Sn in equilibrium with different binary or ternary liquid was made.

Keywords: alloys, solidification, interfaces, thernal conductivity, thermal analysis

1. INTRODUCTION

The solid-liquid interfacial energy, σ_{SL}, is recognized to play a key role in a wide range of metallurgical and materials phenomena from wetting [1] and sintering through to phase transformations and coarsening [2]. Thus, a quantitative knowledge of σ_{SL} values is necessary. However, the determination of σ_{SL} is difficult. Since 1985, a technique for the quantification of solid-liquid interfacial energy from the grain boundary groove shape has been used [3-18]. Observation of groove shape in a thermal gradient can be used to determine the interfacial energy, independent of the grain boundary energy because the interface near the groove must always satisfy

$$\Delta T_r = \left[\frac{1}{\Delta S^*}\right]\left[\left(\sigma_{SL}+\frac{d^2\sigma_{SL}}{d\theta_1^2}\right)\kappa_1+\left(\sigma_{SL}+\frac{d^2\sigma_{SL}}{d\theta_2^2}\right)\kappa_2\right] \quad (1)$$

where ΔT_r is the curvature undercooling, ΔS^* is the entropy change per unit volume, θ_1 and θ_2 refer the orientations of interfaces, κ_1 and κ_2 are the mean curvatures of the interfaces. When the solid-liquid interfacial energy is isotropic, Eq. (1) becomes

$$\Delta T_r = \frac{\sigma_{SL}}{\Delta S^*}\left(\frac{1}{r_1}+\frac{1}{r_2}\right) \quad (2)$$

where r_1 and r_2 are the principal radii of the curvature of the surface. For the case of a planar grain boundary intersecting a planar solid-liquid interface, $r_2=\infty$ and the Eq. (2) becomes

$$\Gamma = r\Delta T_r = \frac{\sigma_{SL}}{\Delta S^*} \quad (3)$$

where Γ is the Gibbs-Thomson coefficient. This equation is called the Gibbs-Thomson relation [13].

At present the most powerful experimental method to measure solid-liquid interfacial energy is the grain boundary groove method. This method is based on the direct application of the Gibbs-Thomson equation and can be applied to measure σ_{SL} for multi-component systems as well as pure materials, for opaque materials as well as transparent materials,

*Corresponding author: kesli@erciyes.edu.tr

for any observed grain boundary groove shape and for any value of the thermal conductivity ratio of the equilibrated liquid phase to solid phase, $R=K_L/K_S$ where K_S is the thermal conductivity of the solid phase and K_L is the thermal conductivity of the liquid phase.

Sn is an important constituent in solder alloys because it wets and adheres to many common base metals at temperatures considerably below their melting temperatures. Sn-based alloys are used in some delicate soldering for electronic equipments. They are also used in computer and other fields of industry [19]. Properties such as stable microstructure, light weight, corrosion resistance, high strength and good castability make Sn-Mg alloys promising materials for different industrial applications. Although the interest in Sn-Mg alloys started in the early 1930s [20], there has recently been strong research interest in the application of Sn- and Mg-based alloys in various branches of technology. Sn-Mg based alloys are commonly used for bearing materials, anodic materials in Li ion batteries etc. [21]. Zn is one of the major alloying elements added to Sn-Mg alloy to improve mechanical property and corrosion resistance [22]. Therefore Sn-Mg-Zn ternary system is one of the important systems in the family of Sn-based alloys and it is worth studying in details. More knowledge about its structural and mechanical properties at different temperatures may be helpful in industrial applications.

Although the phase diagram of the Sn-Mg-Zn ternary system has been determined [22] as shown in Fig. 1, some of its thermo-physical properties such as solid-liquid interfacial energy, Gibbs-Thomson coefficient, grain boundary energy and thermal conductivity of the solid and liquid phases for Sn-Mg-Zn ternary alloy have not yet been fully determined. These thermo-physical properties could be used by those making comparisons between experimentally observed solidification morphology and predictions from theoretical models. Thus, the aim of the present work was to determine the thermal conductivity, Gibbs-Thomson coefficient, solid-liquid interfacial energy and grain boundary energy for solid Sn in Sn-Mg-Zn ternary alloy.

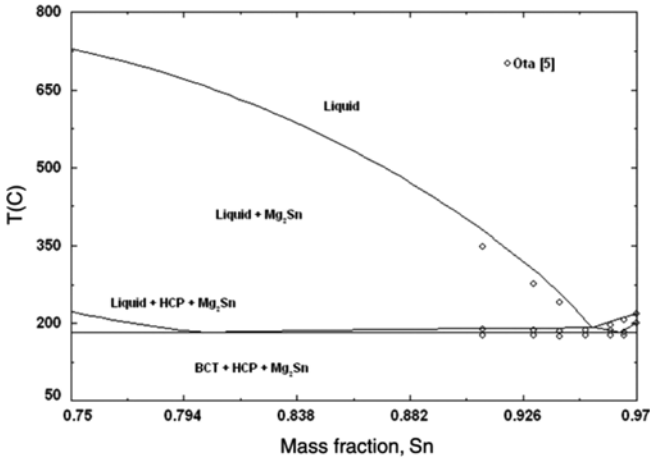

Fig. 1. The phase diagram of Sn-Mg-Zn system for 3 wt% Zn [22].

2. EXPERIMENTAL PROCEDURES

2.1. Sample production

In order to observe the equilibrated grain boundary groove shapes in opaque materials, Gündüz and Hunt [13] designed a radial heat flow apparatus. Maraşlı and Hunt [14] improved the experimental apparatus for higher temperatures. The details of the apparatus and experimental procedures are given in Refs. [13-17]. In the present work, a similar apparatus was used to observe the grain boundary groove shapes in the Sn-Mg-Zn eutectic system.

It is necessary to consider what happens during the annealing period. Consider a binary eutectic system. If the alloy composition (X_0) is near the eutectic composition ($X_0 \cong X_E$) above the eutectic temperature, a binary eutectic system consists of liquid. If this system is held in a very stable temperature gradient there will be no liquid droplets behind the solid phases and two solid phases (a, b) can grow together on the eutectic structure.

In the present study, the composition of the alloy was chosen as Sn-4.59 at% Mg-5.12 at% Zn to grow a single solid Sn phase on the eutectic cast structure in a short annealing time from the phase diagram of Sn-Mg-Zn alloy [22]. The Sn-4.59 at% Mg-5.12 at% Zn alloy was prepared in a vacuum furnace by using 99.80% Sn, 99.98% Mg and 99.99% Zn. After stirring, the molten alloy was poured into a graphite crucible held in a specially constructed casting furnace at approximately 50 K above the melting temperature of the alloy. The molten alloy was then directionally solidified from bottom to top to ensure that the crucible was completely full. The sample was then placed in the radial heat flow apparatus.

The sample was heated from its center by a single heating wire and the outside of the sample was kept constant to an accuracy of ± 0.01 K at 273 K (0 degrees Celsius) by using a *Poly Science digital 9102* model heating/refrigerating circulating bath to maintain a constant radial temperature gradient on the sample. A thin liquid layer (1-2 mm thick) was melted around the central heating wire and the specimen was annealed in a very stable temperature gradient over a long period. During the annealing period, the liquid droplets move radially towards the hot zone of the sample by temperature gradient zone melting and the single solid phase can grow on the eutectic cast phase. If the temperature difference between solidus and liquids lines is high, the freezing range will be larger and the equilibrating (annealing) time will be long. The equilibrating (annealing) time for Sn-4.59 at% Mg-5.12 at% Zn alloy was 4 days. During the annealing period, the temperature in the specimen and the vertical temperature variations on the sample were continuously recorded by the stationary thermocouples and a moveable thermo-

couple, respectively, by using a data logger via computer. The input power was also recorded periodically. The temperature in the sample was kept stable to about ± 0.03 K for up to 4 days. At the end of the annealing time the specimen was rapidly quenched by turning off the input power which was sufficient to get a well-defined solid-liquid interface, because the liquid layer around the central heating wire was very thin (typically less than 0.5-1 mm).

2.2. Measurements of the coordinates of equilibrated grain boundary groove shapes

The quenched sample was cut transversely into lengths of typically 25 mm, and transverse sections were ground flat with 180 grit SiC paper. Grinding and polishing were then carried out by following a standard route.

The equilibrated grain boundary groove shapes were then photographed with an *Olympus DP12* type CCD digital camera placed on top of an *Olympus BX51* type light optical microscope. A graticule (200 × 0.01 = 2 mm) was also photographed using the same objective. The photographs of the equilibrated grain boundary groove shapes and the graticule were superimposed on one another using *Adobe PhotoShop 8.0* version software so that accurate measurement of the groove coordinate points on the groove shapes could be made.

2.3. Geometrical correction for the groove coordinates

The coordinates of the cusp, x, y should be measured using the coordinates x, y, z where the x axis is parallel to the solid-liquid interface, the y axis is normal to the solid-liquid interface and the z axis lies at the base of the grain boundary groove. Maraşlı and Hunt [14] devised a geometrical method to make appropriate corrections to the groove shapes and the details of the geometrical method are given in Ref. [14].

The coordinates of the equilibrated grain boundary groove shapes were measured with an optical microscope, to an accuracy of ±10 μm, by following Maraşlı and Hunt's geometrical method so that appropriate corrections to the shape of the grooves could be deduced [14]. The uncertainty in the measurements of the equilibrated grain boundary groove coordinates is 0.1%.

2.4. Measurements of the thermal conductivity of solid and liquid phases

The thermal conductivity ratio of the equilibrated eutectic liquid phase (Sn-8.12 at% Mg-4.97 at% Zn) to the solid Sn phase, $R = K_{L(\text{eutectic liquid})} / K_{S(Sn)}$, must be known or measured to evaluate the Gibbs-Thomson coefficient with the present numerical method. The radial heat flow method is an ideal technique for measuring the thermal conductivity of the solid phase. The thermal conductivity of the solid Sn phase is also needed to evaluate the temperature gradient in the solid phase. In the radial heat flow method, a cylindrical sample

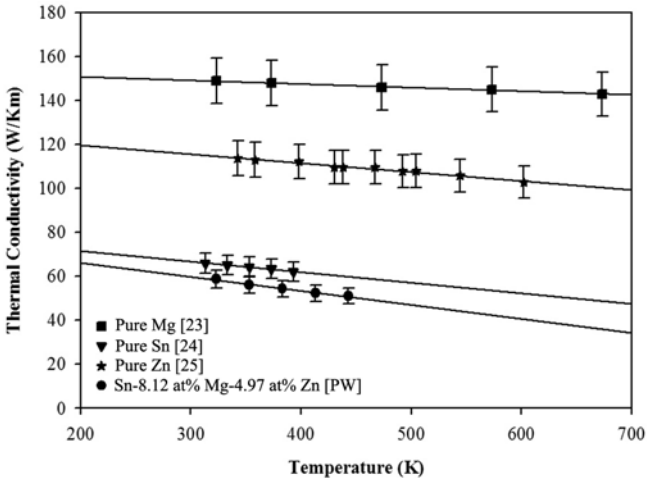

Fig. 2. Thermal conductivity of eutectic solid phase (Sn-8.12 at% Mg-4.97 at% Zn) versus temperature in Sn-Mg-Zn system.

was heated by using a single heating wire in alumina tube along the axis at the center of the sample and the sample was kept in a temperature gradient for a period to achieve a steady-state condition. At the steady-state condition, the temperature gradient of the solid phase in the cylindrical specimen is given by Fourier's law

$$G_S = \frac{dT}{dr} = -\frac{Q}{2\pi r l K_S} \tag{4}$$

where Q is the total input power, r is the distance of the solid-liquid interface to the center of the sample, l is the length of the heating wire which is constant and K_S is the thermal conductivity of the solid phase. Integration of Eq. (4) gives

$$K_S = a_0 \frac{Q}{T_1 - T_2} \tag{5}$$

where $a_0 = \ln(r_2/r_1)/2\pi l$ is an experimental constant, r_1 and r_2 ($r_2 > r_1$) are the fixed distances from the central axis of the specimen, T_1 and T_2 are the temperatures at the fixed positions, r_1 and r_2. Eq. (5) could be used to obtain the thermal conductivity of the solid phase by measuring the difference in temperature between two fixed points for a given power level provided that the vertical temperature variation is minimum or zero.

The thermal conductivity of the eutectic solid (Sn-8.12 at% Mg-4.97 at% Zn) was measured with the radial heat flow apparatus. Sufficient amounts of metallic alloys were melted to produce an ingot of approximately 100 mm in length and 30 mm in diameter in a vacuum furnace. After the processes was repeated as described in sample production part the specimen was placed in the radial heat flow apparatus.

The specimen was heated from the center using a single heating wire (140-190 mm in length and 2.5 mm in diameter,

Kanthal A-1) in steps of 30 K up to 10 K below the melting temperature of the alloy and the outside of the specimen was cooled to maintain a radial temperature gradient. To obtain a reliable value of thermal conductivity, a larger radial temperature gradient is desired. For this purpose, the gap between the cooling jacket and the specimen was filled with free running sand or graphite dust and the outside of the specimen was kept at 273 K using a heating/refrigerating circulating bath. The length of central heating wire was chosen as 10 mm longer than the length of specimen to make the isotherms parallel to the vertical axis.

The specimen was kept at a steady-state condition for at least two hours at a constant temperature. At steady state, the total input power and the stationary thermocouple temperatures were recorded with a *Hewlett Packard 34401* type multimeter and a *Pico TC-08* data-logger. The temperatures on the different parts of the specimen were measured with mineral insulated, metal sheathed, 0.5 mm in diameter K type thermocouples. A zero or minimum vertical temperature gradient is desired in thermal conductivity measurements. The vertical temperature for each setting was tried to be constant by moving the central heater up and down. After all desired power settings and temperature measurements had been completed during the heating procedure, the cooling procedure was started in the same steps down to room temperature.

Then the sample was removed from the furnace and cut transversely near to the measurement points of thermocouples; after that the specimen was ground and polished for the measurements of r_1 and r_2. The positions of the thermocouples were then photographed with an *Olympus DP12* CCD digital camera placed in conjunction with an *Olympus BX51* type light optical microscope. A graticule (200 × 0.01 = 2 mm) was also photographed using the same objective. The photographs of the positions of the thermocouples and the graticule were superimposed on one another using *Adobe PhotoShop 8.0* software so that accurate measurement of the distances of the stationary thermocouples could be made to an accuracy of ±10 μm. The transverse and longitudinal

Table 1. Thermal conductivities of solid and liquid phases and their ratios at their eutectic temperatures for Sn based alloys.

Alloy	Phases	Melting Temperature (K)	K (W/Km)	$R=K_L/K_S$
Sn-Mg-Zn [PW]	Eutectic Liquid (Sn-8.12 at% Mg-4.97 at% Zn)	456	41.82	0.83
	Eutectic Solid (Sn-8.12 at% Mg-4.97 at% Zn)		50.39	
	Eutectic Liquid (Sn-8.12 at% Mg-4.97 at% Zn)	456	41.82	0.70
	Solid (Sn)		59.44	
Sn-Bi-Ag [26]	Eutectic Liquid (Sn-10 at% Bi-2 at% Ag)	480.65	22.96	0.72
	Eutectic Solid (Sn-10 at% Bi-2 at% Ag)		31.89	
	Eutectic Liquid (Sn-10 at% Bi-2 at% Ag)	480.65	22.96	0.65
	Solid (Sn-8.4 at% Bi)		35.50	
Sn-Bi-In [27]	Liquid (In-21.23 at% Bi-19.04 at% Sn)	332.15	28.07	0.96
	Solid (In-21.23 at% Bi-19.04 at% Sn)		29.24	
	Liquid (In-21.23 at% Bi-19.04 at% Sn)	332.15	28.07	0.89
	Solid Sn solution (Sn-40.14 at% In-16.11 at% Bi)		31.56	
Sn-Pb [13]	Liquid (Sn-26.1 at% Pb)	456	32.2	0.80
	Solid (Sn-26.1 at% Pb)		40.1	
Sn-Sb [28]	Peritectic liquid (Sn-7.8 at% Sb)	518.65	34.42	0.85
	Peritectic solid (Sn-7.8 at% Sb)		40.50	
	Peritectic liquid (Sn-7.8 at% Sb)	518.65	34.42	1.07
	Solid (Sn-41.4 at% Sb)		31.98	
	Liquid (Sn-5 at% Sb)	518.65	22	0.51
	Solid (Sn-5 at% Sb)		43	
Sn-Zn [29]	Eutectic liquid (Sn-8.9 wt% Zn)	472	21.10	-
	Eutectic solid (Sn-8.9 wt% Zn)		35.74	
Sn-Cu [30]	Eutectic liquid (Sn-1.3 at% Cu)	500.15	44.76	0.76
	Eutectic solid (Sn-1.3 at% Cu)		58.90	
	Eutectic liquid (Sn-1.3 at% Cu)	500.15	44.76	0.75
	Solid (Sn)		59.88	
Sn-Ag-In [35]	Eutectic liquid (Sn-4.4 at% Ag-2.1 at% In)	490.65	42.50	0.68
	Eutectic solid (Sn-4.4 at% Ag-2.1 at% In)		62.50	
	Eutectic liquid (Sn-4.4 at% Ag-2.1 at% In)	490.65	42.50	0.73
	Sn solution (Sn-2.1 at% In)		58.40	

PW: Present Work

sections of the specimen were examined for porosity, crack and casting defects to make sure that these would not introduce any error to the measurements.

The thermal conductivity of the eutectic solid versus temperature is plotted in Fig. 2. A comparison of the thermal conductivity of the eutectic solid with the thermal conductivity of Mg [23], Sn [24] and Zn [25] is also given in Fig. 2. The value of K_S for the Sn-Mg-Zn eutectic solid at the eutectic temperature was obtained to be 50.39 W/Km, by extrapolating to the eutectic temperature as shown in Fig. 2.

It is not possible to measure the thermal conductivity of the liquid phase with the radial heat flow apparatus since a thick liquid layer (10 mm) is required. A layer of this size would certainly have led to convection. If the thermal conductivity ratio of the liquid phase to the solid phase is known and the thermal conductivity of the solid phase is measured at the melting temperature, the thermal conductivity of the liquid phase can then be evaluated. The thermal conductivity ratio can be obtained during directional growth with a Bridgman-type growth apparatus. The details of the experimental procedure are given in Refs. (13)-(17).

The thermal conductivity ratio of the eutectic liquid (Sn-8.12 at% Mg-4.97 at% Zn) to the eutectic solid (Sn-8.12 at% Mg-4.97 at% Zn), $R=K_{L(eutectic)}/K_{S(eutectic)}$, was experimentally measured as 0.83 with a Bridgman-type growth apparatus. The thermal conductivity of the Sn-8.12 at% Mg-4.97 at% Zn eutectic solid at the eutectic temperature was also measured to be 50.39 W/Km. The thermal conductivity of the eutectic liquid phase was then determined to be 41.82 W/Km. Thus, the thermal conductivity ratio of the equilibrated eutectic liquid phase to the solid Sn phase, $R= K_{L(eutectic\ liquid)}/K_{S(Sn)}$, is also found to be 0.70 by using the values of thermal conductivity of the eutectic liquid and thermal conductivity of the solid Sn 59.44 W/Km [24]. The thermal conductivities of the solid and liquid phases for solid Sn and Sn-Mg-Zn eutectic solid and their ratios used in the determination of the Gibbs-Thomson coefficient are also given in Table 1.

A comparison of the values of K_S and K_L for Sn-Mg-Zn alloy obtained in the present work with the values of K_S and K_L for Sn based alloys [13,26-30] obtained in previous works is given in Table 1. As can be seen from Table 1, the values of K_S and K_L for Sn, obtained in present work agree very well with the values of K_S and K_L obtained in previous works.

2.5. Measurement of temperature gradient in the solid phase

The temperature gradient of the solid phase must be determined for each grain boundary groove shape. This was done by measuring the input power, the length of heating wire, the position of the solid-liquid interface and the value of K_S for solid Sn phase at the eutectic point. By using these measured values in Eq. (4), the temperature gradient can be determined for each grain boundary groove shapes. The total fractional uncertainty in the measurement of the temperature gradient is about 6.5% [14].

3. RESULTS AND DISCUSSIONS

3.1. Determination of Gibbs-Thomson coefficient

If the thermal conductivity ratio of the equilibrated liquid phase to the solid phase, the coordinates of the grain boundary groove shape and the temperature gradient of the solid phase are known, the Gibbs-Thomson coefficient (Γ) can be obtained using the numerical method described in detail in Ref. (13). The experimental error in the determination of the Gibbs-Thomson coefficient is the sum of experimental errors in the measurement of the temperature gradient, thermal conductivity and groove coordinates. Thus the total error in the determination of the Gibbs-Thomson coefficient is estimated to be about 7% [14].

The Gibbs-Thomson coefficients for solid Sn in equilibrium with the eutectic liquid (Sn-8.12 at% Mg-4.97 at% Zn) were determined with the present numerical model by using ten equilibrated grain boundary groove shapes. Typical grain boundary groove shapes for solid Sn in equilibrium with the eutectic liquid are shown in Fig. 3.

The values of Γ for solid Sn are given in Table 2. The average value of Γ from Table 2 is $(8.3 \pm 0.6) \times 10^{-8}$ Km for solid Sn in equilibrium with the Sn-Mg-Zn eutectic liquid.

3.2. Determination of entropy of fusion per unit volume

In order to determine the solid-liquid interfacial energy it is also necessary to know the entropy of fusion per unit volume, ΔS^* for solid phase. The entropy of fusion per unit volume, ΔS^* for a two-component system is [31].

$$\Delta S^* = \frac{RT_m}{m_L}\frac{(C_{S\infty}-C_{L\infty})}{(1-C_{L\infty})C_{L\infty}}\frac{1}{V_S} \quad (6)$$

$C_{L\infty}$ and $C_{S\infty}$ are the equilibrium concentrations of solid

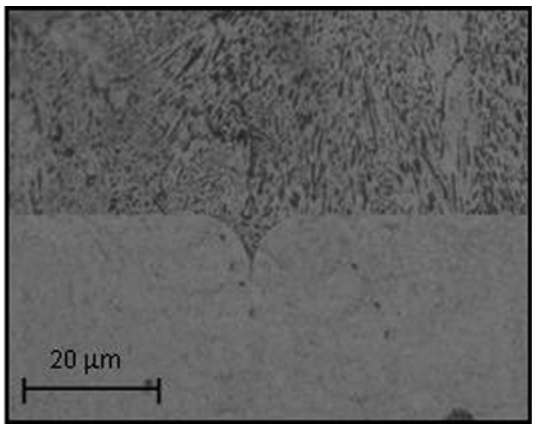

Fig. 3. Typical grain boundary groove shape for solid Sn in equilibrium with the Sn-8.12 at% Mg-4.97 at% Zn eutectic liquid.

Table 2. The Gibbs-Thomson coefficients for solid Sn in equilibrium with the Sn-8.12 at% Mg-4.97 at% Zn eutectic liquid. The subscripts LHS and RHS refer to left hand side and right hand side of the groove respectively.

Grove No	$G_k \times 10^2$ (K/m)	α^o	β^o	Gibbs-Thomson Coefficient	
				$\Gamma_{LHS} \times 10^{-8}$ (Km)	$\Gamma_{RHS} \times 10^{-8}$ (Km)
a	5.63	12.6	12.0	8.3	8.4
b	5.55	12.3	11.2	8.5	8.6
c	4.32	14.3	12.3	8.3	8.1
d	4.52	10.9	12.0	8.1	8.5
e	4.16	11.8	11.5	8.5	8.3
f	4.25	12.6	12.6	8.4	8.8
g	4.29	10.3	11.5	8.0	8.4
h	4.56	11.2	10.6	8.0	8.2
i	4.17	14.5	12.0	8.3	8.4
j	4.45	14.3	12.8	8.4	8.5
				$\overline{\Gamma} = (8.3 \pm 0.6) \times 10^{-8}$ Km	

α is the angle between x' and x axes.
β is the angle between y' and y axes.

and liquid phases for a flat interface, respectively, m_L is the liquidus slope, R is the gas constant, T_m is the equilibrating temperature and V_S is the molar volume of solid phase. The entropy change per unit volume is given by

$$\Delta S^* = \frac{\Delta H_f}{T_m}\frac{1}{V_S} = \frac{\Delta H_f}{T_m} \tag{7}$$

where ΔH_f^* is the enthalpy of fusion per unit volume. The enthalpy of fusion also known as (latent) heat of fusion is the change in enthalpy resulting from heating a given quantity of a substance to change its state from a solid to a liquid. The temperature at which this occurs is the melting point.

The enthalpy of fusion is a latent heat, because during melting the introduction of heat cannot be observed as a temperature change, as the temperature remains constant during the process. The latent heat of fusion is the enthalpy change of any amount of substance when it melts. When the heat of fusion is referenced to a unit of mass, it is usually called the specific heat of fusion, while the molar heat of fusion refers to the enthalpy change per amount of substance in moles.

The liquid phase has a higher internal energy than the solid phase. This means energy must be supplied to a solid in order to melt it and energy is released from a liquid when it freezes, because the molecules in the liquid experience weaker intermolecular forces and so have a higher potential energy (a kind of bond-dissociation energy for intermolecular forces).

The molar volume of solid is expressed as

$$V_S = V_c N_a \frac{1}{n} \tag{8}$$

where V_c is the volume of the unit cell, N_a is the Avogadro's number and n is the number of molecules per unit cell.

The enropy of fusion for solid Sn solution in the Sn-Cu system was determined as 1.3×10^6 J/Km^3 by Kaygısız *et al.* [30] at the equilibrating temperature of 500 K. Solid Sn solution phases in the Sn-Cu and Sn-Mg-Zn systems have same crystal structures and the enthalpy of fusion per unit volume for solid Sn solutions in both Sn-Cu and Sn-Mg-Zn systems should be close to each other. Therefore, the entalpy of fusion per unite volume for solid Sn solution, $\Delta H_f^* = \Delta H_f^{Sn}/V_S$ is obtained to be 6.5×10^8 J/m^3 from Gibbs-Thomson equation by multiplying the value of 1.3×10^6 J/Km^3 with the equilibrating temperature of 500 K. Thus, the entropy of fusion per unit volume for solid Sn solution in the Sn-Mg-Zn ternary system is determined to be 1.42×10^6 J/Km^3 from equation (6) at the equilibrated melting temperature of 456 K by dividing the enthalpy of fusion per unit volume (6.5×10^8 J/m^3) to the equilibrated melting temperature of 456 K. Some physical properties for solid Sn in equilibrium with Sn-8.12 at% Mg-4.97 at% Zn eutectic liquid are given in Table 3. The error in the determination of entropy of fusion per unit volume is estimated to be about 5% [13,14,32].

3.3. Evaluation of the solid-liquid interfacial energy

If the values of Γ and ΔS^* are known, the value of the solid-liquid interfacial energy, σ_{SL}, can be evaluated from Eq. (3). The solid-liquid interfacial energy of the solid Sn in equilib-

Table 3. Some physical properties for solid Sn in equilibrium with Sn-8.12 at% Mg-4.97 at% Zn eutectic liquid

Alloy	Solid Phase	Liquid Phase	Eutectic Melting Temperature K	ΔS^* (J K^{-1}m^{-3})
Sn-Cu	Sn	Sn-1.3 at% Cu	500.15 [30]	1.3×10^6 [30]
Sn-Mg-Zn	Sn	Sn-8.12 at% Mg-4.97 at% Zn	456 [22]	1.4×10^6

rium with the Sn-Mg-Zn eutectic liquid (Sn-8.12 at% Mg-4.97 at% Zn) was calculated as $(118.5 \pm 14.2)\times10^{-3}$ J m^{-2} by using the values of Γ and ΔS^*. The experimental error in the determination of solid-liquid interfacial energy is the sum of experimental errors of the Gibbs-Thomson coefficient and the entropy change of fusion per unit volume. Thus, the total experimental error of the solid-liquid interfacial energy evaluation in the present work is estimated to be about 12%.

3.4. Grain boundary energy

If the grains on either side of the grain boundary are in the same phase then the grain boundary energy can be expressed by

$$\sigma_{gb} = 2\sigma_{SL}\cos\theta \quad (9)$$

where $\theta = (\theta_A + \theta_B)/2$ is the angle that the solid-liquid interfaces make with the y axis. The angles, θ_A and θ_B were obtained from the cusp coordinates, x, y using a Taylor expansion for parts at the base of the groove. According to Eq. (1), the value of σ_{gb} should be smaller or equal to twice the solid-liquid interfacial energy, i.e. $\sigma_{gb} \leq 2\sigma_{SL}$.

The value of the grain boundary energy for the solid Sn was found to be $(225.1 \pm 29.3)\times10^{-3}$ J m^{-2} by using the values of the σ_{SL} and θ in Eq. (9). The estimated error in the determination of θ angles was found to be 1%. Thus the total experimental error in the resulting grain boundary energy is about 13%.

Interfacial energy anisotropy is considered to play a critical role in many phase transformations. The determination of the effects of anisotropy on the interfacial energy is difficult. In the literature, there are no theoretical or experimental available data for the anisotropy of the interfacial energy of the solid Sn phase. Thus the solid-liquid interfacial energy is assumed to be isotropic. A comparison of the values of the Gibbs-Thomson coefficient (Γ), solid-liquid interfacial energy (σ_{SL}) and grain boundary energy (σ_{gb}) for solid Sn phase measured in the present work with the values of Γ, σ_{SL}, σ_{gb} for solid Sn phases in different alloy systems obtained in previous works is given in Table 4. As can be seen from Table 4, the resulting values of σ_{SL} and σ_{gb} for solid Sn in the Sn-Mg-Zn system agree well with the values of σ_{SL} and σ_{gb} determined in previous works [13,26,27,30,33-35] for solid Sn phases. From the comparison, it can be concluded that for solid Sn in equilibrium with different liquid, the Gibbs-Thomson coefficient seems to be constant and does not depend on the composition of liquid but the solid-liquid interfacial energy changes slightly with a composition of the liquid at a constant temperature.

In order to estimate the interfacial energy an empirical relationship between the interfacial energy and melting enthalpy change was proposed by Turnbul [3] and is expressed as

$$\sigma_{SL} = \frac{\tau \Delta H_M}{V_S^{2/3} N_a^{1/3}} \quad (10)$$

where the coefficient τ was found to be 0.45 for metals (especially closely packed metals) and 0.34 for nonmetallic systems at about 20% of undercooling below the melting point [3], ΔH_M is the enthalpy of fusion, V_S is molar volume of the solid phase and N_a is the Avogadro constant. However, subsequent experiments generated substantially larger values of undercooling resulting in larger values of σ_{SL}, indicating that such experiments typically underestimate σ_{SL}, except where there is independent evidence that homogenous rather than heterogeneous nucleation was operative. The other disadvantages

Table 4. A comparison of the values of Γ, σ_{SL} and σ_{gb} and for solid Sn obtained in the present work with the values of Γ, σ_{SL} and σ_{gb} obtained in previous works for similar eutectic alloys

System	Solid phase	Liquid phase	T_M (K)	$\Gamma\times10^{-8}$ (K m)	$\sigma_{SL}\times10^{-3}$ (J m^{-2})	$\sigma_{gb}\times10^{-3}$ (J m^{-2})
Sn-Mg-Zn [PW]	Sn	Eutectic liquid (Sn-8.12 at% Mg-4.97 at% Zn)	456	8.2 ± 0.6	118.5 ± 14.2	225.1 ± 29.3
Sn-Ag-Bi [26]	Sn solution (Sn-8.4 at% Bi)	Eutectic liquid (Sn-10 at% Bi-2 at% Ag)	480.65	8.4 ± 0.6	108.9 ± 13.1	208.2 ± 27.1
Sn-Cu [30]	Sn	Eutectic liquid (Sn-1.30 at% Cu)	500.15	8.7 ± 0.6	113.1 ± 13.6	222.4 ± 28.9
Sn-Ag-Zn [33]	Sn (Sn-0.09 at% Ag-0.4 at% Zn)	Eutectic liquid (Sn-4.0 at% Ag-1.6 at% Zn)	490	8.21 ± 0.7	116.2 ± 15.1	228.1 ± 34.2
Sn-Ag [34]	Sn (Sn-0.09 at% Ag)	Eutectic liquid (Sn-3.84 at% Ag)	494	8.86 ± 0.71	113.41 ± 14.74	222.96 ± 33.4
Sn-Pb [13]	Sn (Sn-1.45 at% Pb)	Eutectic liquid (Sn-26.1 at% Pb)	456	7.85 ± 0.63	132.4 ± 5.0	262.7 ± 36.7
Sn-Ag-In [35]	Sn solution (Sn-2.1 at% In)	Eutectic liquid (Sn-4.4 at% Ag-2.1 at% In)	490.65	8.5 ± 0.6	142.2 ± 17.1	273.0 ± 35.5
Sn-In-Bi [27]	Sn solution (Sn-40.14 at% In-16.1 at% Bi)	Eutectic liquid (In-21.23 at% Bi-19.04 at% Sn)	332.15	7.68 ± 0.39	144.4 ± 14.4	284.6 ± 31.3

PW: Present Work

of deriving σ_{SL} from undercooling experiments were discussed by Jones [4] and Eustathopoulos [5].

As mentioned above, the groove profile method actually measures $\Gamma = \sigma_{SL}/\Delta S^*$ so that value is required for ΔS^* to evaluate σ_{SL}. Substituting Eq. (3) into Eq. (10) gives

$$\Gamma = \tau T_m \left(\frac{V_M}{N_A}\right)^{1/3} = \tau T_m \Omega^{1/3} \quad (11)$$

where Ω is volume per atom.

Gransasy *et al.*, [36] calculated the value of τ from the broken-bond theory. The minimum values of τ for the fcc, hcp, bcc, dc and sc structures were found to be 0.458, 0.458, 0.445, 0.289 and 0.333 respectively, and the maximum value of τ for the fcc, hcp, bcc, dc and sc structures were also found to be 0.592, 0.582, 0.630, 0.500 and 0.577 respectively at the melting temperature. Hoyt *et al*. [12] plotted the Turnbull relationship for many fcc and bcc metals via the capillarity fluctuation method (CFM) and also found the values of τ for the fcc and bcc structures to be 0.55 and 0.29, respectively. More recently, Jones [37] has compared the values of Γ and σ_{SL} measured by groove profile methods with the values of Γ and σ_{SL} measured by other methods and determined the values of τ for metallic binary alloys by using the measured values of Γ. He found the values of τ to range from 0.13 for Al_3Ni to 1.0 for α-Al. According to the values of τ determined by Jones [37], the value of τ changes with the type of material and it might be in the range from 0.13 to 1.0 for the binary metallic materials. In the present work, the average value of τ for solid Sn was obtained to be 0.61 from Eq. (10) by using the determined values of Γ and is in a good agreement with the value of τ calculated from the supercooling experiments of Turnbull [3] for metallic materials.

4. CONCLUSIONS

A radial temperature gradient on the sample was established by heating from the center with a single heating wire and cooling the outside of the sample with a heating/refrigerating circulating bath. The equilibrated grain boundary groove shapes for solid Sn in equilibrium with the Sn-Mg-Zn eutectic liquid were observed from a quenched sample. Some thermophysical properties such as the Gibbs-Thomson coefficient, solid-liquid interfacial energy and grain boundary energy of solid Sn in equilibrium with the Sn-Mg-Zn eutectic liquid were experimentally determined from the observed grain boundary groove shapes. The thermal conductivity of the eutectic solid phase at the eutectic temperature was also determined. All these determined values agree well with the values determined in previous works for solid Sn phases in different systems. In future research, the solid-liquid interfacial energy may also be theoretically determined by recently improved computational simulation methods [38,39] by applying the method to the grain boundary groove shapes.

ACKNOWLEDGEMENTS

This project was supported by Erciyes University Scientific Research Project Unit under Contract No:FDK-2013-4467. The authors would like to thank Erciyes University's Scientific Research Project Unit for their financial support.

REFERENCES

1. N. Eustathopoulos, M. G. Nicholas, and B. Drevet, *Wettability at High Temperatures*, p.148, Pergamon Materials Series, Oxford, Pergamon (1999).
2. J. W. Martin, R. D. Doherty, and B. Cantor, *Stability of Microstructure in Metallic Systems*, p.27, Cambridge University Press, Cambridge (1997).
3. D. Turnbull, *J. Appl. Phys.* **21**, 1022 (1950).
4. D. R. H. Jones, *J. Mater. Sci.* **9**, 1 (1974).
5. N. Eustathopoulos, *Int. Met. Rev.* **28**, 189 (1983).
6. G. F. Bolling and W. A. Tiller, *J. Appl. Phys*. **31**, 1345 (1960).
7. G. E. Nash and M. E. Glicksman, *Phil. Mag.* **24**, 577 (1971).
8. D. R. H Jones and G. A. Chadwick, *J. Cryst. Growth* **11**, 260 (1971).
9. R. J. Schaefer, M. E. Glicksman and J. D. Ayers, *Phil. Mag.* **32**, 725 (1975).
10. S. C. Hardy, *Phil. Mag.* 35, 471 (1977).
11. N. B. Singh, M. E. Glicksman, and *J. Cryst. Growth* **98**, 573 (1989).
12. J. J. Hoyt, M. Asta, T. Haxhimali, A. Karma, R. E. Napolitano, and R. Trivedi, *MRS Bulletin* **29**, 935 (2004).
13. M. Gündüz and J. D. Hunt, *Acta Mater* **33**, 1651 (1985).
14. N. Maraşlı and J.D. Hunt, *Acta Mater*. **44**, 1085 (1996).
15. K. Keşlioğlu and N. Maraşlı, *Mat. Sci. Eng. A-Struct* **369**, 294 (2004).
16. Y. Ocak, S. Akbulut, K. Keşlioğlu, and N. Maraşlı, *J. Phys. D Appl*. **41**, 1 (2008).
17. Y. Ocak, S. Akbulut, K. Keşlioğlu, N. Maraşlı, E. Çadırlı, and H. Kaya, *Chinese Phys. B* **18**(9), 3952 (2009).
18. A. Bulla, C. Carreno-Bodensiek, B. Pustal, R. Berger, A. Bührig-Polaczek, and A. Ludwig, *Metall. and Mater. Trans. A* **38**, 1956 (2007).
19. F. Abd El-Salam, A. M. Abd El-Khalek, R. H. Nada, M. R. Nagy, and R. Abd El-Haseeb, *Mater. Sci. Eng. A* **506**, 135 (2009).
20. G. Derge, A. R. Kommel, and R. F. Mehl, *AIME* **124**, 367 (1937).
21. B. Saatçi, M. Arı, M. Gündüz, S. Türktekin, F. Meydaneri, S. Durmuş, and M. Özdemir, *Continuum Mech. Thermodyn*. **25**, 739 (2013).
22. P. Ghosh, M. Mezbahul-Islam, and M. Medraj, *CALPHAD* **36**, 28 (2012).
23. Y. S. Touloukian, R. W. Powell, C. Y. Ho, and P. G. Klemens, *Thermal Conductivity Metallic Elements and Alloys*, vol. 1, p.205, New York, Washington (1970).

24. Y. S. Touloukian, R. W. Powell, C. Y. Ho, and P. G. Klemens, *Thermal Conductivity Metallic Elements and Alloys*, vol. 1, p.389, New York, Washington (1970).
25. Y. S. Touloukian, R. W. Powell, C. Y. Ho, and P. G. Klemens, *Thermal Conductivity Metallic Elements and Alloys*, Vol. 1, p.498, New York, Washington (1970).
26. E. Öztürk, S. Aksöz, K. Keşlioğlu, and N. Maraşlı, *Mater. Chem. and Phys.* **139**, 153 (2013).
27. S. Akbulut, Y. Ocak, N. Maraşlı, K. Keşlioğlu, H. Kaya, and E. Çadırlı, *Mater. Charact*. **60**, 183 (2009).
28. Y. Kaygısız, Y. Ocak, S. Aksöz, K. Keşlioğlu, and N. Maraşlı, *Thermochim. Acta* **520**, 25 (2011).
29. B. Saatçi, N. Maraşlı, and M. Gündüz, *Thermochim. Acta* **454**, 128 (2007).
30. Y. Kaygısız, Y. Ocak, S. Aksöz, N. Maraşlı, K. Keşlioğlu, E. Çadırlı, and H. Kaya, *Chem. Phys. Lett.* **484**, 219 (2010).
31. E. Öztürk, S. Aksöz, K.Keşlioğlu, and N. Maraşlı, *Metall. and Mater. Trans A*, **45A**, 1161 (2014).
32. J. W. Christian, *The Theory of Transformations in Metals and Alloys Part I, 2nd. ed.* p.180, Oxford, Pergamon (1975).
33. S. Engin, U. Böyük, and N. Maraşlı, *Curr. App. Phys*. **11**, 1060 (2011).
34. S. Engin, U. Böyük, and N. Maraşlı, *J. Alloy Compd*. **488**, 138 (2009).
35. Y. Ocak, S. Aksöz, N. Maraşlı, and K. Keşlioğlu, *Chem. Phys. Lett.* **496**, 263 (2010).
36. L. Garanasy, M. Tegze, and A. Ludwig, *Mat. Sci. Eng. A-Struct* **133**, 577 (1991).
37. H. Jones, *Mater. Trans. A* **A38**, 1563 (2007).
38. B. Li and H. Qin, *In Proceedings of the 19th*, *Pacific Conference on Computer Graphics and Applications*, p.49, Pacific Graphics (2011).
39. B. Li and H. Qin, *Computer Graphics*, **36**, 329 (2012).